Meteosat Surface Albedo (MSA)

Product User's Manual

and Format Guide

Document	**:**	**EUM/FG/13**
MSA algorithm release	**:**	MSA VERSION 2.1
Document issue	**:**	**May 2010**

Contents

List of Acronyms

AOT	Aerosol Optical Thickness
BRF	Bidirectional Reflectance Factor
BHR	Bi-Hemispherical Reflectance
DHR	Directional Hemispherical Reflectance
ECMWF	European Centre for Medium range Weather Forecasts
HDF	Hierarchical Data Format
JRC	Joint Research Centre
MSA	Meteosat Surface Albedo
MTP	Meteosat Transition Programme
SDS	Scientific DataSets
SSP	Sub-Satellite Point
SSR	Sensor Spectral Response
TOA	Top Of Atmosphere
TOMS	Total Ozone Mapping Spectrometer
VIS	VISible

1 Introduction

1.1 Scope

This document describes the Meteosat Surface Albedo (MSA) product version 2.1 generated on the MTP MPEF re-processing environment at EUMETSAT. The original version of this algorithm has been developed at the Space Applications Institute of DG JRC of the European Commission. It is maintained and improved by EUMETSAT.

1.2 Document structure

Section (2) provides an overview of the MSA retrieval algorithm which assumptions are given in Section (3). The product content is described in Section (5). The conversion of the MSA product in broadband albedo is given in Section (4.3). Changes with respect to the original MSA version are listed in Section (6.1) and Section (6.3) respectively.

1.3 Contact Point

All enquiries relating to this document or to the Meteosat Archive in general should be directed to:

UMARF Customer Enquiries
EUMETSAT
Am Kavalleriesand 31
D-64295 Darmstadt
Germany
Telephone: +49 6151 807 377
Electronic mail: ops@eumetsat.int

1.4 MSA product ordering

The MSA algorithm has been used to process meteosat observations from 1982 (Meteosat-2) up to 2006 (Meteosat-7) over the 0° position. Since summer 1998, EUMETSAT is operating a second geo-stationary satellite over the Indian ocean. These data are also been processed with the MSA algorithm. The product can be ordered from our web page at the following URL:

http://archive.eumetsat.org/umarf/

You need to be a registered user to order products. In the list of products, the MSA product is identified as the MTP Mean Surface Albedo 0100. Make sure your select the format you want.

2 Outline of the retrieval procedure

2.1 Overview

The cornerstone of the surface albedo algorithm relies on the exploitation of the temporal sampling of geostationary observations as if it were an instantaneous angular sampling. The algorithm accumulates therefore VIS band observations for each pixel during one day to form a measurement vector (Section 2.2). The radiative state of the observed medium, *i.e.*, the atmosphere and the underlying surface, are defined by a set of state variables (Section 2.3) that need to be inferred from space observations or ancillary source of information. The value of these state variables is retrieved through the inversion of a forward radiative transfer model (Section 2.4) against the measurement vector, minimising the differences between observations and simulations, normalised by the respective measurement system error (Sections 2.5 and 2.6). The lack of spectral information and the radiometric noise limit the possibility to unequivocally discriminate among the various solutions that could fit the measurement vector for a given level of confidence. This level of confidence depends on the size of the measurement vector that can change from pixel to pixel according to cloud and illumination conditions. Hence, a probability is assigned to each solution that specifically depends upon the number of degrees of freedom and the value of the cost function (Section 2.7). The estimation of the retrieved parameter error relies on a statistical analysis of the solution ensemble equally satisfying the inversion scheme given the measurement error (Section 2.8). A 10-day temporal compositing technique is applied to maximise the spatial coverage of cloud free pixels (Section 2.9). Finally the retrieved surface state variables are used to derive the Directional Hemispherical Reflectance (DHR) corresponding to a fixed Sun position of 30° together with its respective error. The estimated retrieval error and the probability of the solution are the two key elements that should permit a meaningful comparison of surface albedo derived from different radiometers.

During the retrieval process, it is assumed that (*i*) surface and atmospheric scattering properties are constant along the day, (*ii*) continental aerosol type applied everywhere and all year long, (*iii*) surface anisotropy can be represented with the simple Bidirectional Reflectance Factor (BRF) model proposed by Rahman et al. (1993) and finally (*iv*) the reciprocity principle is valid over terrestrial surfaces at a spatial resolution of a few kilometers (Lattanzio et al. 2006).

2.2 Measurement vector

Meteosat image line (row) and pixel (column) acquisition results from a combination of the main mirror rotation and satellite spin. These images are acquired by the Meteosat Visible and Infrared Imager (MVIRI) in three channels that includes a solar band (referred to as the VIS band), ranging from 0.4 up to 1.1 μm. This VIS band is systematically calibrated against simulated radiances over stable bright desert targets (Govaerts et al. 2004). The measurement vector $\boldsymbol{y}_m$ consists of time series of VIS band top-of-atmosphere (TOA) BRF accumulated under different illumination angles Ω_s during the course of one day.

This vector contains only clear-sky observations, cloudy observations are disregarded with the high frequency filtering method proposed by Pinty et al. (2000b). Obvious cloudy conditions are screened by setting a threshold value equal to 0.6 on the TOA BRF measurements. In order to eliminate unscreened events such as remaining clouds, topography shadows, errors in the data geo-

rectification process, and/or significant sub-daily variations in the aerosol load and type, a Data Consistency Procedure produces an angularly smooth but coherent TOA BRF series which accounts for hot spot conditions. This procedure checks the consistency of the pre-screened TOA BRF values by attempting to fit the data series against a generic parametric BRF model, namely a Modified version of the RPV model ((Engelsen et al. 1996)). An iterative process eliminates the observed BRF value exhibiting the largest absolute departure with respect to the model prediction. The result of the fit, χ^2_{DCP}, between the modelled TOA BRF and the remaining measurements provides an estimation of the filtering process cost, accounting for an uncertainty σ_{DCP} between the data and the model. A pixel is further processed only if it contains at least six cloud free daily observations.

The size of this vector, noted N_y, can clearly change from place to place and time to time according to the duration of the day, the cloud condition and finally the actual number of available observations. A minimum of six clear sky observations per day are necessary to perform an inversion.

2.3 State vector

The state vector represents the ensemble of radiative parameters that describes the observed medium in the VIS spectral band. It is actually divided into two categories. The first one, noted $\boldsymbol{x}$, represents the parameters that are retrieved through the inversion of the measurement vector, namely the Equivalent Aerosol Optical Thickness (EAOT) τ and three parameters $\{\rho_0, \Theta, k\}$ that characterise the state of the surface anisotropy represented by the RPV parametric BRF model proposed by Rahman et al. (1993). This model writes

$$\rho_s(z_0, \Omega_s, \Omega_v; \rho_0, \Theta, k) = \rho_0 \breve{\rho}_s(z_0, \Omega_s, \Omega_v; \Theta, k) \tag{1}$$

where Ω_s and Ω_v are the illumination and viewing direction and z_0 denotes the bottom of the atmosphere. ρ_0 and $\breve{\rho}_s(z_0, \Omega_s, \Omega_v; \Theta, k)$ describe the amplitude and the angular field of the surface BRF, respectively. The elements of the state vector $\boldsymbol{x}$ that specifically represent the surface properties, *i.e.*, $\{\rho_0, \Theta, k\}$, are noted $\boldsymbol{x}_s$. Due to the lack of available spectral information, it is not possible to retrieve all variables that characterise the radiative state of the observed medium. Those parameters defining the state of the observed medium but that are not part of the retrieved parameters are referred to as the *model* parameters and are noted $\boldsymbol{b}$. In the present case, $\boldsymbol{b}$ is composed of the water vapour and ozone total column concentration noted respectively U_{H2O} and U_{O3}. The total column water vapour is taken from the European Centre for Medium-Range Weather Forecasts (ECMWF) analysed data and the total column ozone from the Total Ozone Mapping Spectrometer (TOMS) observations (McPeters 1996).

Parameters	**Values**
k	0.4, 0.5, 0.6, 0.7, 0.8, 0.9, 1.0
Θ	-0.30, -0.25, -0.20, -0.15, -0.10, -0.05, 0.00
τ	0.1, 0.2, 0.3, 0.4, 0.6, 0.8, 1.0

Table 1: Discretisation values of the k, Θ and τ parameters.

2.4 Forward model

A complete description of the forward model can be found in Pinty et al. (2000a). Only its final form is reported here for the sake of clarity. This model assumes the separation of the gaseous absorption from the scattering processes which is conceptually similar to the separation of the atmosphere into two distinct layers. The first one, hosting the atmospheric scattering processes, ranges from levels z_0 up to z_a. The gaseous absorption takes place in the second one which ranges between levels z_a and z_s. Under this formalism, the TOA BRF observed values, $y(z_s, \Omega_s(t), \Omega_v)$, acquired at time t with geometrical illumination $\Omega_s(\mu_s, \phi_s)$ and viewing conditions and $\Omega_v(\mu_v, \phi_v)$, can be approximated by:

$$y(z_s, \Omega_s(t), \Omega_v; \boldsymbol{x}, \boldsymbol{b}) = T_g(\mu_s(t), \mu_v; \boldsymbol{b})\Big(\rho_a(z_a, \Omega_s(t), \Omega_v; \tau) + \rho_0\, \breve{\rho}_s(z_a, \Omega_s(t), \Omega_v; \tau, \boldsymbol{x}_s)\Big) \quad (2)$$

where $T_g(\mu_s(t), \mu_v; \boldsymbol{b})$ is the transmission factor for absorbing gases, $\rho_a(z_a, \Omega_s(t), \Omega_v; \tau)$ is the intrinsic reflectance of the scattering layer, ρ_0 is the amplitude of the surface BRF, and $\breve{\rho}_s(z_a, \Omega_s(t), \Omega_v; \tau, \boldsymbol{x}_s)$ is the angular field of the BRF at level z_a, *i.e.*, at the top of the scattering layer.

To speed-up the inversion process, the function $\breve{\rho}_s(z_a, \Omega_s(t), \Omega_v; \tau, \boldsymbol{x}_s)$ is pre-computed for an ensemble of pre-defined values of τ, k and Θ listed in Table (1). The corresponding ρ_0 values are estimated for all combinations of these pre-defined atmospheric and surface conditions with

$$\rho_0 = \frac{\sum_{t=1}^{N_y} \left[\boldsymbol{y}_m(t)/T_g(\mu_s(t), \mu_v; \boldsymbol{b}) - \rho_a(z_a, \Omega_s(t), \Omega_v; \tau)\right]}{\sum_{t=1}^{N_y} \breve{\rho}_s(z_a, \Omega_s(t), \Omega_v; \tau, \boldsymbol{x}_s)}. \quad (3)$$

2.5 Cost function definition

Finding the value of $\boldsymbol{x}$ that minimises the difference between the measurement vector $\boldsymbol{y}_m$ and the forward model $y(\boldsymbol{x}, \boldsymbol{b})$ is obtained for a χ^2 metrics defining the cost function. Neglecting the angular notation, this function writes

$$\chi^2 = \sum_{t=1}^{N_y} \left(\frac{\boldsymbol{y}_m(t) - y(t; \boldsymbol{x}, \boldsymbol{b})}{\sigma_{\boldsymbol{y}}(t)}\right)^2 \quad (4)$$

where $\sigma_{\boldsymbol{y}}(t)$ is the measurement error. The number of degrees of freedom of χ^2 is defined as $\nu = N_y - N_x$ where N_x is the number of elements of the state vector $\boldsymbol{x}$, *i.e.*, four in the present retrieval system.

2.6 Measurement error characterisation

2.6.1 General definition

The measurement error $\sigma_{\boldsymbol{y}}$ includes both the instrumental uncertainty and the forward model approximations. The radiometric error has several different contributions. The first one is of course the radiometric noise of the instrument resulting from the dark current and other undesired electronics effects. The digitalisation level is also considered as a source of error. It is equal to 64 levels (6 bits data) for the Meteosat-2 observations and 256 levels (8 bits data) for Meteosat-7. As daily observations are assumed to be virtual instantaneous measurements, it is necessary to translate image geo-location inaccuracies into equivalent radiometric error. Similarly, the actual aerosol load is

subject to change during the daily accumulation of the measurement vector. Indeed, the longer this accumulation period, *i.e.*, the elapsed time between the first and the last clear-sky observation, the higher the probability that the aerosol load varies. Possible daily variations of the aerosol load are thus considered as measurement errors. An aerosol daily autocorrelation function is introduced to convert these changes into an equivalent radiometric error. Hence, the total measurement error $\sigma_{\boldsymbol{y}}(t)$ of a pixel acquired at time t is dynamically estimated as the contributions of (*i*) the detector radiometric noise $\sigma_{\boldsymbol{I}}$, (*ii*) the digitalisation error $\sigma_{\boldsymbol{D}}$, (*iii*) the rectification uncertainty $\sigma_{\boldsymbol{R}}$, (*iv*) the aerosol daily autocorrelation $\sigma_{\boldsymbol{A}}$ and (*v*) the forward model error σ_F. Assuming that these terms are not correlated, the total measurement error is expressed by

$$\sigma_{\boldsymbol{y}}(t) = \sqrt{\sigma^2_{\boldsymbol{I}}(t) + \sigma^2_{\boldsymbol{D}}(t) + \sigma^2_{\boldsymbol{R}}(t) + \sigma^2_{\boldsymbol{A}}(t) + \sigma^2_{\boldsymbol{F}}(t)}. \tag{5}$$

The terms $\sigma_{\boldsymbol{I}}$, $\sigma_{\boldsymbol{D}}$ and $\sigma_{\boldsymbol{R}}$ characterise the observation errors whereas the terms $\sigma_{\boldsymbol{A}}$ and $\sigma_{\boldsymbol{F}}$ represent the model assumption and forward modelling errors. The uncertainty on the model parameters $\boldsymbol{b}$ are not explicitly estimated but are included in the term $\sigma_{\boldsymbol{F}}$. The dependence of the surface parameter characterisation on the actual position of the angular sampling is not included in the measurement error. A previous study has shown that errors that might results from an insufficient angular sampling remain small compared to $\sigma_{\boldsymbol{y}}$ (Lattanzio et al. 2006).

2.6.2 Detector noise σ_I

During the processing of a row image conversion into a rectified image, referred to as level 1.5 data, an equalisation process takes place between the histogram of the two detectors to minimise any difference in the detector sensitivity. Hence, the radiometric error of the VIS band includes the contribution of the detector noise and their sensitivity difference, *i.e.*,

$$\sigma_{\boldsymbol{I}}(t) = \boldsymbol{y}_m(t)\,\frac{\sigma_{K_{1.5}}(t)}{K(t) - \overline{K}_0(t)} \tag{6}$$

where K is the digital count value, $\overline{K}_0$ is the mean space count value and $\sigma_{K_{1.5}}$ the level 1.5 radiometric noise, *i.e.*, after the rectification and detector equalisation process. For MVIRI, the radiometric noise writes

$$\sigma_{K_{1.5}}(t) = \boldsymbol{y}_m(t)\,\sqrt{\frac{1}{8}\sum_{c=1}^{8}\left(\sigma_{\overline{K}_0}(c)\right)^2 + \left(\frac{\overline{K}_{01}(t) - \overline{K}_{02}(t)}{2}\right)^2} \tag{7}$$

where $\sigma_{\overline{K}_0}(c)$ is the mean space count standard deviation of one detector over one corner. $\overline{K}_{0n}$ is the mean space value of detector n linearly averaged over the four space corners. The first term of the right hand side accounts for individual detector noise whereas the second term represents the difference between the detectors.

2.6.3 Digitalisation noise σ_D

This term accounts for the digitalisation of the observed radiances in count values K on b bits. The corresponding digitalisation uncertainty is

$$\sigma_{\boldsymbol{D}}(t) = \boldsymbol{y}_m(t)\,\frac{0.5\,D_f}{K(t) - \overline{K}_0(t)} \tag{8}$$

where $D_f = 2^8/2^b$, 256 digitalisation levels (8 bits data) being taken as the reference.

2.6.4 Rectification noise σ_R

As daily observations are assumed to be virtual instantaneous measurements, it is necessary to account for image rectification inaccuracies that can occur during the course of the day. For a pixel located at a position (p_1, p_2), these inaccuracies are converted into an equivalent radiometric noise

$$\sigma_{\boldsymbol{R}}(t, p_1, p_2) = \boldsymbol{y}_m(t) \frac{1}{K(t, p_1, p_2) - \overline{K}_0(t)} \sqrt{\left(\frac{\partial K(t, p_1, p_2)}{\partial p_1}\sigma_{p_1}(t)\right)^2 + \left(\frac{\partial K(t, p_1, p_2)}{\partial p_2}\sigma_{p_2}(t)\right)^2} \tag{9}$$

where $\sigma_{p_1}(t)$ and $\sigma_{p_2}(t)$ are the root mean square error between land marks identified in the rectified image and their actual earth location along the p_1 and p_2 direction respectively.

2.6.5 EAOT autocorrelation error σ_A

The longer the duration between the first and the last clear sky images, the higher the probability that the aerosol load actually varies. Analysis of AErosol RObotic NETwork (AERONET) (Holben et al. 1998) time series revealed that stable daily aerosol load typically corresponds to a temporal autocorrelation of 0.95 between two successive Meteosat observations. These changes introduce perturbations in the observed signal since the daily time series is assumed to have been instantaneously acquired. Such deviation from the algorithm assumptions can be converted into an equivalent radiometric error. Assuming that the daily aerosol load variations are represented by a first order auto regressive model, the EAOT τ at slot $t + dt$ can be expressed as a function of EAOT at slot t

$$\tau(t + dt) = \alpha\tau(t) + \beta(t) = \tau(t) + (\alpha - 1)\tau(t) + \beta(t) \tag{10}$$

where α is the autocorrelation and β a random noise with a mean equal to zero. In the same way, we have

$$\begin{aligned}
\tau(t + 2dt) &= \alpha(\alpha\tau(t) + \beta(t)) + \beta(t + 2dt) && (11)\\
\tau(t + 3dt) &= \alpha(\alpha(\alpha\tau(t) + \beta(t)) + \beta(t + 2dt)) + \beta(t + 3dt) && (12)\\
\tau(t + h) &= \alpha^h\tau(t) + \alpha^{h-1}\beta(t) \cdots + \beta(t + h) && (13)
\end{aligned}$$

Assuming that $\beta = 0$ and neglecting the changes in the illumination direction between two successive slots, the equivalent radiometric error at slot $t + h$ is equal to

$$y(\tau(t + h)) = y(\tau(t) + (\alpha - 1)\tau(t)) \tag{14}$$

or, assuming a local linear behaviour of $y(\tau(t))$

$$y(\tau(t)) = y(\tau(t)) + \frac{\partial y(\tau(t))}{\partial \tau}((\alpha^h - 1)\tau(t)) \tag{15}$$

The change $\partial y(\tau)/\partial\tau((\alpha^h - 1)\tau(t))$ from slot t to $t + h$ is thus an undesired perturbation that can be considered as a radiometric noise of the measurement system. The corresponding relative autocorrelation radiometric error for any slot $t_m = m + h$ writes

$$\sigma_{\boldsymbol{A}}(t) = \frac{\partial y(\tau(t))}{\partial \tau}\left((\alpha^h - 1)\tau(t_m)\right) \tag{16}$$

where $t_m = (t_{min} + t_{max})/2$ with t_{min} and t_{max} are respectively the first and last slot not under-illuminated of the day. Large aerosol load variations are not covered by this method.

2.6.6 The forward model error σ_F

As seen in Section (2.4), the state variables k, Θ, τ have been discretized at intervals $\Delta k, \Delta\Theta, \Delta\tau$ to speed-up the retrieval process. This discretisation is responsible for an error that writes

$$\sigma_{\boldsymbol{F}}(t) = y(t;\boldsymbol{x},\boldsymbol{b})\sqrt{\left(\frac{\partial y(t;\boldsymbol{x},\boldsymbol{b})}{\partial k}\frac{\Delta k}{2}\right)^2 + \left(\frac{\partial y(t;\boldsymbol{x},\boldsymbol{b})}{\partial \Theta}\frac{\Delta \Theta}{2}\right)^2 + \left(\frac{\partial y(t;\boldsymbol{x},\boldsymbol{b})}{\partial \tau}\frac{\Delta \tau}{2}\right)^2} \quad (17)$$

The discretisation steps $\Delta k, \Delta\Theta, \Delta\tau$ should be small enough so that the condition $\sigma_{\boldsymbol{F}}(t) \ll \sqrt{\sigma^2_{\boldsymbol{I}}(t) + \sigma^2_{\boldsymbol{D}}(t) + \sigma^2_{\boldsymbol{R}}(t)}$ is verified and the discretisation error neglected. However, this condition is not always true as it not possible to explore a very large number of solutions, limiting thereby the discretisation steps. It is thus necessary to account for the source of error $\sigma_{\boldsymbol{F}}$. Equation (17) is estimated once and for all to avoid its explicit computation for each pixel and slot.

2.7 Estimation of the most likely solution

The solution of the coupled surface-aerosol scattering problem is obtained dynamically during the retrieval based on the pre-computation of the function $\breve{\rho}_s(z_a, \Omega_s(t), \Omega_v; \tau, \boldsymbol{x}_s)$ for a set of pre-defined Θ, k and τ values listed in Table (1). For each of these pre-defined solutions $\boldsymbol{x}(j)$, the corresponding value of $\rho_0(j)$ is estimated first with Equation (3). The values of $\chi^2(\boldsymbol{x}(j))$ given by Equation (4) are calculated next for each of these solutions j. As the number of degrees of freedom of $\chi^2(\boldsymbol{x}(j))$ can vary from pixel to pixel, it is not possible to establish *a priori* a unique minimum threshold value below which a value of $\chi^2(\boldsymbol{x}(j))$ constitutes an acceptable solution. Assuming a Gaussian distribution of the summation terms of the cost function (Equation 4), the distribution of $\chi^2(\boldsymbol{x})$ can be represented by an incomplete Gamma function. The probability to find a $\chi^2(\boldsymbol{x}(j))$ smaller than a given threshold value χ^2_a is expressed by

$$P_a(\chi^2(\boldsymbol{x}(j)) < \chi^2_a, \nu) = 1 - \frac{1}{2^{\nu/2}\Gamma(\nu/2)}\int_0^{\chi^2_a} e^{-a/2}t^{\nu/2-1}da \quad (18)$$

where Γ is the Gamma function. From this expression, it is possible to define the probability that the model parameters fit the observations by chance. A small probability should be interpreted as a poor agreement between the observations and the forward model. As the number of degrees of freedom decreases, the χ^2_a value decreases for a constant confidence in the solution.

Let us now define $\chi^2(P_a, \nu)$, the value of χ^2 corresponding to a probability P_a for ν degrees of freedom and $\mathcal{L}_a$ the ensemble of solutions $\{\boldsymbol{x}(l)\}$ satisfying the condition

$$\mathcal{L}_a = \{\chi^2(\boldsymbol{x}(j)) < \chi^2(P_a, \nu)\}. \quad (19)$$

Only solutions with a probability higher than a defined threshold value P_a are considered as acceptable. In this ensemble of valid solutions $\mathcal{L}_a$, the most likely solution $\hat{\boldsymbol{x}}$ is chosen as the one with the smallest χ^2 value, except if the dispersion of acceptable solutions is too large (Pinty et al. 2000b). In that case, the selection of the most likely solution is the one with the smallest χ^2 value whose ρ_0 value falls in the interval $\rho_0 \in \overline{\rho}_0 \pm \sigma_{\overline{\rho}_0}$ where $\overline{\rho}_0$ is weighted mean value of the $\rho_0(l)$ values in $\mathcal{L}_a$ and $\sigma_{\overline{\rho}_0}$ the weighted standard error estimated with

$$\sigma_{\overline{\rho}_0} = t_{P_a/2}(L_a - 1)\sqrt{\sum_{l=1}^{L_a}\kappa_t(l)\,(\rho_0(l) - \overline{\rho}_0)^2} \quad (20)$$

where L_a is the number of solutions in the ensemble $\mathcal{L}_a$ and $t_{P_a/2}(L_a - 1)$ is the Student coefficient for the 2-tails distribution with $L_a - 1$ degrees of freedom. The weight κ_t is equal to

$$\kappa_t(l) = \frac{\chi^2(P_a, \nu) - \chi^2(\boldsymbol{x}(l))}{\sum_{l=1}^{L_a} \left(\chi^2(P_a, \nu) - \chi^2(\boldsymbol{x}(l))\right)}. \tag{21}$$

The maximum probability P_a that defines the ensemble of acceptable solutions could not be selected arbitrarily but constrained by the measurement uncertainty. This relationship is examined in the next Section.

2.8 Retrieval error estimation

The surface parameter error estimation allows the assessment of the DHR retrieval uncertainty and therefore supports a meaningful temporal analysis of surface albedo data sets derived from different instruments. In this analysis, systematic errors such as those resulting from calibration uncertainties are not taken into account in the retrieval process.

A statistical approach is proposed here for the estimation of the error $\sigma_{\hat{\boldsymbol{x}}}$ of the retrieved solution $\hat{\boldsymbol{x}}$. Due to the measurement error $\sigma_{\boldsymbol{y}}$, a solution $\hat{\boldsymbol{x}}'$ close to the actual solution $\hat{\boldsymbol{x}}$ could not necessarily be considered significantly different. Following a similar reasoning as in Section (2.7), the error $\sigma_{\boldsymbol{y}}$ defines thus an ensemble of solutions $\mathcal{L}_{\sigma_y}$ that are not discriminable, *i.e.*, that are significantly different. This ensemble of solutions $\{\boldsymbol{x}(m)\}$ can be defined by the condition

$$\mathcal{L}_{\sigma_y} = \{\chi^2(\boldsymbol{x}) < \chi^2(P_{\sigma_y}, \nu)\}. \tag{22}$$

where P_{σ_y} is the corresponding probability, yet to be defined. Conceptually, the threshold value $\chi^2(P_{\sigma_y}, \nu)$ should be equal to $\chi^2(\hat{\boldsymbol{x}} + \sigma_{\hat{\boldsymbol{x}}})$. The average value of $\chi^2(\hat{\boldsymbol{x}} + \sigma_{\hat{\boldsymbol{x}}})$ can be approximated by (Govaerts and Lattanzio 2007)

$$\langle \chi^2(\hat{\boldsymbol{x}} + \sigma_{\hat{\boldsymbol{x}}}) \rangle \approx \frac{\langle y(\hat{\boldsymbol{x}} + \sigma_{\hat{\boldsymbol{x}}}) - \boldsymbol{y}_m \rangle}{\sigma_{\boldsymbol{y}}} = \chi^2(\hat{\boldsymbol{x}}) + \langle \chi^2(\hat{\boldsymbol{x}}) \rangle \tag{23}$$

where $\langle \chi^2(\hat{\boldsymbol{x}}) \rangle$ is the average value of $\chi^2(\hat{\boldsymbol{x}})$ over many processed pixels. The ensemble of solutions $\boldsymbol{x}(m) \in \mathcal{L}_{\sigma_y}$ that are not discernable with respect to the measurement error $\sigma_{\boldsymbol{y}}$ is thus defined by the condition

$$\mathcal{L}_{\sigma_y} = \{\chi^2(\boldsymbol{x}(m)) \leq \chi^2(\hat{\boldsymbol{x}}) + t_{P_{\alpha/2}}(\infty)\ \langle \chi^2(\hat{\boldsymbol{x}}) \rangle\}. \tag{24}$$

Let us now examine the relationship between P_a and P_{σ_y}. All elements in the ensemble $\mathcal{L}_{\sigma_y}$ should constitute acceptable solutions which translates into the condition $\mathcal{L}_{\sigma_y} \subseteq \mathcal{L}_a$. The probability P_a has thus to be chosen to satisfy the inequality

$$\chi^2(P_{\sigma_y}, \nu) = \chi^2(\hat{\boldsymbol{x}}) + t_{P_a}(\infty)\ \langle \chi^2(\hat{\boldsymbol{x}}) \rangle\ \leq\ \chi^2(P_a, \nu). \tag{25}$$

P_{σ_y} constitutes thus the maximum acceptable probability which determines the minimum acceptable $\chi^2(P_{\sigma_y}, \nu)$ value as a function of the measurement error $\sigma_{\boldsymbol{y}}$. In order to increase the spatial coverage of the generated products, this probability is decreased when no solution satisfies Equation (24), *i.e.*, when $\mathcal{L}_{\sigma_y}$ is empty. Pixels processed with this decreased probability should be considered as backup solutions and carefully interpreted. Hence, P_{σ_y} is used as a quality indicator of the solution reliability accounting for the measurement error and the actual number of available observations.

The error $\sigma_{\hat{\boldsymbol{x}}}$ is defined by the distribution of the ensemble of solutions $\boldsymbol{x}(m) \in \mathcal{L}_{\sigma_y}$ with

$$\sigma^2_{\hat{\boldsymbol{x}}} = t_{P_a}(L_{\sigma\boldsymbol{y}} - 1)\sigma^2_{\boldsymbol{x}} + \left(\frac{\partial y(t;\hat{\boldsymbol{x}},\boldsymbol{b})}{\partial \hat{\boldsymbol{x}}}\frac{\Delta\hat{\boldsymbol{x}}}{2}\right)^2 \tag{26}$$

where $L_{\sigma\boldsymbol{y}}$ is the number of solutions in $\mathcal{L}_{\sigma_y}$, $\sigma^2_{\boldsymbol{x}}$ is the standard deviation of $\boldsymbol{x}(m)$. The second term of the right hand side part of Equation (26) represents the error due to the discretisation of the $\boldsymbol{x}$ space. This term is equal to zero for the ρ_0 parameter.

2.9 Temporal compositing

The objective of the temporal compositing is to maximise the number of clear sky processed pixels during a 10-day period. This compositing relies on the selection of the most representative solution over the accumulation period. The most obvious way is to select the solution with the best fit accounting for the actual number of degrees of freedom. Hence, the most representative solution $\overline{\hat{\boldsymbol{x}}}$ within a 10-day period is the one with the highest probability. However, as clouds tend to increase the signal received at the satellite level, selecting the solution with the smallest $\widehat{\rho}_0$ will tend to minimise the impact of undetected clouds. Thus, if two or more solutions have the same probability, the one with the lowest $\widehat{\rho}_0$ is selected.

Surface albedo is generally not expected to undergo important changes during a 10-day period so that the repetition of the same measurement might be assumed from day to day. Under these conditions, the temporal stability of the solution during a compositing period should increase the confidence in the retrieved product. The error of the most representative solution $\overline{\hat{\boldsymbol{x}}}$ writes

$$\sigma_{\overline{\hat{\boldsymbol{x}}}} = \frac{t_{P_a/2}(N_T - 1)}{\sqrt{N_T}}\sqrt{\sum_{d=1}^{N_T}\hat{\kappa}_T(d)(\hat{\boldsymbol{x}}(d) - \overline{\hat{\boldsymbol{x}}})^2} \tag{27}$$

where N_T is the number of days with an acceptable solution during the compositing period. The normalised weight $\hat{\kappa}_T(d)$ is estimated as

$$\hat{\kappa}_T(d) = \frac{1}{P(\hat{\boldsymbol{x}}(d))} \tag{28}$$

where $P(\hat{\boldsymbol{x}}(d))$ is the probability of the solution $\hat{\boldsymbol{x}}$ of day d. It is thus expected that the uncertainty of the retrieved solution decreases as the number of days increases except for those places that are subject to drastic temporal changes in surface albedo as is in case of wild fires (Govaerts et al. 2002). When only one likely solution has been found during the compositing period, $\sigma_{\overline{\hat{\boldsymbol{x}}}}$ is set equal to $\sigma_{\hat{\boldsymbol{x}}}$.

2.10 Surface albedo error estimation

The DHR is defined as

$$\text{DHR}(\theta_0 = 30^\circ) = \int_{2\pi}\rho_s(z_0,\Omega_s,\Omega';\overline{\hat{\boldsymbol{x}}}_s)d\Omega' = \overline{\widehat{\rho}_0}\int_{2\pi}\breve{\rho}_s(z_0,\Omega_s,\Omega';\overline{\hat{k}},\overline{\widehat{\Theta}})d\Omega' \tag{29}$$

and is calculated for a sun position fixed at 30°. Assuming that the errors on $\overline{\widehat{\boldsymbol{x}}}_s$ are not correlated, the non-systematic error on the estimation of the DHR is expressed with

$$\sigma_{\text{DHR}} \approx \sqrt{\left(\frac{\partial \text{DHR}}{\partial \rho_0}\sigma_{\overline{\widehat{\rho}}_0}\right)^2 + \left(\frac{\partial \text{DHR}}{\partial \Theta}\sigma_{\overline{\widehat{\Theta}}}\right)^2 + \left(\frac{\partial \text{DHR}}{\partial k}\sigma_{\overline{\widehat{k}}}\right)^2}. \tag{30}$$

Since the variable of integration, *i.e.*, the solid angle,is not derived, the derivation and integration operators can be exchanged, and Equation (30) writes

$$\begin{aligned} \sigma_{\text{DHR}} = \\ \Bigg[\left(\int_{2\pi} \breve{\rho}_s(z_0, \Omega_s, \Omega'; \overline{\widehat{k}}, \overline{\widehat{\Theta}}) d\Omega' \, \sigma_{\overline{\widehat{\rho}}_0}\right)^2 + \\ \left(\int_{2\pi} \frac{\partial \rho_s(z_0, \Omega_s, \Omega'; \overline{\widehat{\boldsymbol{x}}}_s)}{\partial \Theta} \text{d}\Omega' \, \sigma_{\overline{\widehat{\Theta}}}\right)^2 + \\ \left(\int_{2\pi} \frac{\partial \rho_s(z_0, \Omega_s, \Omega'; \overline{\widehat{\boldsymbol{x}}}_s)}{\partial k} \text{d}\Omega' \, \sigma_{\overline{\widehat{k}}}\right)^2 \Bigg]^{1/2}. \end{aligned} \tag{31}$$

Additional information on this error estimation can be found in Govaerts and Lattanzio (2007).

2.11 Product generation

For each 10-day compositing periods, the following two physical quantities are calculated:

- The Directional Hemispherical Reflectance (DHR) estimated with Equation (29) using the solution $\overline{\widehat{\boldsymbol{x}}}$.
- The isotropic Bi-Hemispherical Reflectance $\text{BHR}_\bullet$ estimation with

  $$BHR_\bullet = \overline{\widehat{\rho}}_0 \, \alpha_0(\overline{\widehat{k}}, \overline{\widehat{\Theta}}) \tag{32}$$

  Refer to Pinty et al. (2000a) for the definition of α_0.

3 Algorithm assumptions

The approach relies on a daily accumulation of Meteosat observations acquired at about 20 different illumination conditions to characterise the scattering properties of the surface and the atmosphere, assuming that

1. Surface and atmospheric scattering properties are constant along the day.
2. A US62 vertical profile and continental aerosol type applied everywhere and all year long.
3. Surface anisotropy can be represented with the simple BRF model proposed by Rahman et al. (1993).
4. The reciprocity principle is valid over terrestrial surfaces at a spatial resolution of a few kilometers.

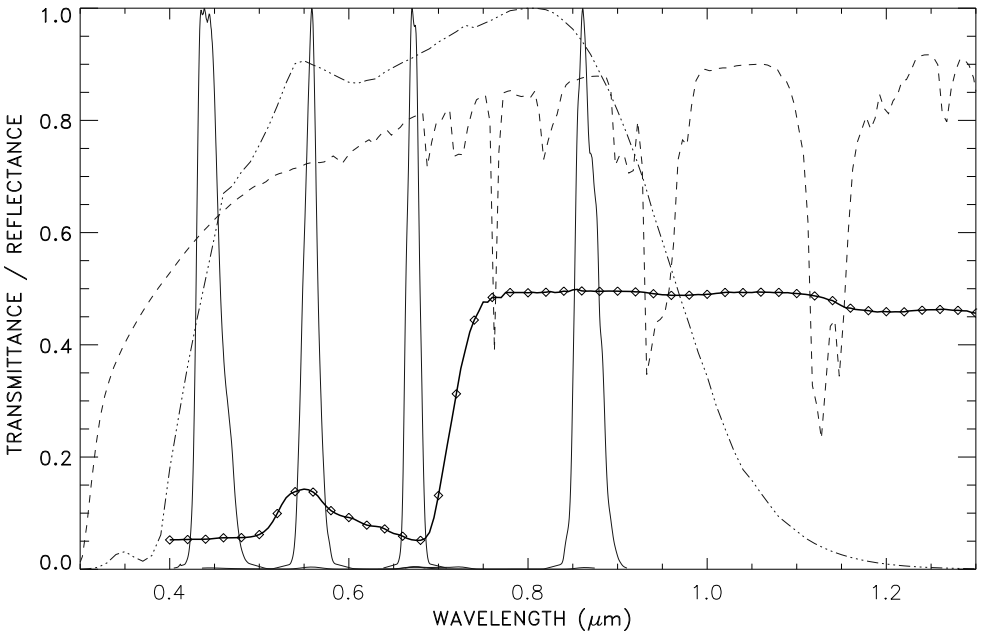

Figure 1: Sensor spectral response of Meteosat-7 VIS band (dash-dotted line) and of Terra - MISR bands (solid lines). The dotted line represents the total transmittance in a US standard atmosphere with an aerosol optical thickness of 0.2 at 0.55μm. The solid line with the $\diamond$ symbols illustrates typical vegetated surface reflectance.

4 Algorithm limitations and MSA product usage

4.1 RTM in the VIS spectral band

The radiometer on-board the Meteosat First Generation (MFG) satellites acquires radiances twice per hour in a single large solar spectral band ranging approximately from 0.4 μm up to 1.1 μm, referred to as the VIS band (Fig. 1). This interval contains some strong gas absorption bands and is also subject to aerosol scattering-absorption processes whose magnitude varies with wavelength. Consequently, the decoupling between absorption and scattering processes, an assumption implemented in the retrieval algorithm to speed-up the atmospheric correction scheme, introduces some inaccuracies when the spectral integration is performed over such a large interval. Additionally, vegetated surface reflectance exhibits quite strong and fast spectral variations over this spectral region as a consequence of the differences in the radiation transfer regimes occurring on both sides of 0.7 μm that is, mainly governed by absorption (scattering) at wavelengths shorter (larger) than 0.7 μm (Fig. 1). These spectral variations can hardly be explicitly taken into account in the atmospheric correction scheme as observations occur only in one single band under different illumination conditions. Consequently, surface albedo derived from geostationary satellite observations in the VIS band with the MSA algorithm is subject to some systematic biases depending on the shape of the surface spectra, the aerosol load and absorbing gas concentration. Under such circumstances, these spectral effects occurring within the VIS band need to be corrected prior performing the spectral conversion *per se* or any other quantitative analysis of the MSA product.

4.2 Cloud contamination

The cloud detection method, described in Pinty et al. (2000b), based on the temporal analysis of the TAO BRF, does not perform optimally when the cloud cover remains stable during an entire day. Consequently, some surface albedo pixel might still be contaminated by undetected clouds. Conservative filtering applied on the probability field and DHR estimated error could be applied to minimize cloud contamination. It is thus recommended to restrict the analysis of the DHR or BHR$_\bullet$ fields to those pixels with a probability P_a larger or 80% or 90% and a σ_{DHR}/DHR relative error over 10 days smaller than 50

4.3 Conversion to broadband albedo

The method to transform the DHR derived in the Meteosat VIS band DHR$_{\text{VIS}}$ in shortwave broadband albedo DHR$_{\text{BB}}$ is described in Govaerts et al. (2006). This relationship is defined with a third order polynomial which writes

$$\text{DHR}_{\text{BB}} = a + b\,\text{DHR}_{\text{VIS}} + c\,(\text{DHR}_{\text{VIS}})^2 + d\,(\text{DHR}_{\text{VIS}})^3 \tag{33}$$

The theoretical coefficients a to d, and estimated error, are taking the following the values according to the Meteosat number:

Met	a	σ_a	b	σ_b	c	σ_c	d	σ_d
2	-0.001373	0.000929	1.151864	0.010025	-1.050935	0.034711	0.982703	0.036453
3	-0.005766	0.001059	1.379440	0.012034	-1.937480	0.043114	1.978280	0.046822
4	-0.008710	0.001044	1.515150	0.012562	-2.437060	0.047526	2.666630	0.054438
5	-0.008631	0.001101	1.570897	0.013324	-2.704288	0.050545	2.962255	0.057886
6	-0.008631	0.001101	1.570897	0.013324	-2.704288	0.050545	2.962255	0.057886
7	-0.008631	0.001101	1.570897	0.013324	-2.704288	0.050545	2.962255	0.057886

For the conversion of the BHR$_\bullet$, the theoretical coefficients and estimated errors are:

Met	a	σ_a	b	σ_b	c	σ_c	d	σ_d
2	-0.010763	0.001114	1.237110	0.011794	-1.372230	0.039732	1.29425	0.040739
3	-0.015561	0.001282	1.469920	0.014277	-2.287270	0.049667	2.31498	0.052521
4	-0.020920	0.001298	1.629200	0.015319	-2.863820	0.056389	3.09297	0.063063
5	-0.025204	0.001445	1.414329	0.016393	-2.061527	0.057746	2.08778	0.061947
6	-0.025204	0.001445	1.414329	0.016393	-2.061527	0.057746	2.08778	0.061947
7	-0.025204	0.001445	1.414329	0.016393	-2.061527	0.057746	2.08778	0.061947

The application of these coefficients on the DHR or BHR$_\bullet$ values derived on the VIS band of MVIRI of the various Meteosat first generation satellites should provide a temporal consistent time

series of broadband surface albedo. However, inaccuracies in the pre-launch characterisation of the sensor spectral response (SSR) might jeopardize the validity of the theoretical spectral conversion factors. Govaerts (1999) already reported inconsistencies in the original SSR values of the VIS band onboard Meteosat-5 and -6, proposing the use of the Meteosat-7 one for these two satellites. Hence, these coefficients could be safely applied to albedo values derived from observations acquired by the Meteosat-5 to -7 satellites. For data acquired by Meteosat-2 to -4, evaluation analysis in still ongoing. Recently, Loew and Govaerts (2010) found some temporal discrepancies when these coefficients are used for the spectral conversion of Meteosat-2 to -4. These authors developed an empircal method to derive the spectral coefficients for the Meteosat-2 to -4 satellites. it is currently recommended to use these empirical coefficients instead of the theoretical ones:

The empircal coefficients a to d for the DHR conversion are taking the following the values according to the Meteosat number (Loew and Govaerts 2010):

Met	a	b	c	d
2	-2.95364443e-05	1.22636437e+00	-1.45464587e+00	1.27798259e+00
3	-2.95364443e-05	1.32036722e+00	-1.52968502e+00	1.25365901e+00
4	-2.95364589e-05	1.22655797e+00	-1.07426369e+00	8.96015048e-01
5	-2.95364443e-05	1.25341415e+00	-1.09384084e+00	8.89843404e-01
6	-2.95364443e-05	1.30573940e+00	-1.31526375e+00	1.05711114e+00
7	-2.95364589e-05	1.26273489e+00	-1.11476350e+00	9.00940299e-01

For the conversion of the BHR$_\bullet$, the empircal coefficients are:

Met	a	b	c	d
2	-2.85976712e-05	9.81895685e-01	-8.48408699e-01	7.43798614e-01
3	-2.85976712e-05	1.09896255e+00	-1.07471538e+00	9.11732554e-01
4	-2.85976712e-05	1.00361478e+00	-6.55005634e-01	6.47315860e-01
5	-2.85976712e-05	1.04928327e+00	-7.66418219e-01	7.47902989e-01
6	-2.85976712e-05	1.15992260e+00	-1.13301563e+00	9.98916626e-01
7	-2.85976712e-05	1.03751910e+00	-6.88233614e-01	7.00615168e-01

4.4 BHR$_\bullet$ error estimation

The BHR$_\bullet$ (see Equation 32) error is currently not stoed in the distributd product. This error can be calculated with the following expression:

$$\sigma_{\text{BHR}_\bullet} \approx \sqrt{\sigma^2_{\bar{\hat{\rho}}_0} + \left(\frac{\partial \alpha_0(\bar{\hat{k}}, \bar{\hat{\Theta}})}{\partial k}\, \sigma_{\bar{\hat{k}}}\right)^2 + \left(\frac{\partial \alpha_0(\bar{\hat{k}}, \bar{\hat{\Theta}})}{\partial \Theta}\, \sigma_{\bar{\hat{\Theta}}}\right)^2} \tag{34}$$

where α_0 is tabulated with the following value:

h	Θ	k	α_0
0.15	-0.30	0.40	3.29568
0.15	-0.30	0.50	2.91138
0.15	-0.30	0.60	2.62286
0.15	-0.30	0.70	2.40092
0.15	-0.30	0.80	2.22700
0.15	-0.30	0.90	2.08885
0.15	-0.30	1.00	1.97802
0.15	-0.25	0.40	3.15165
0.15	-0.25	0.50	2.77600
0.15	-0.25	0.60	2.49365
0.15	-0.25	0.70	2.27618
0.15	-0.25	0.80	2.10550
0.15	-0.25	0.90	1.96964
0.15	-0.25	1.00	1.86037

h	Θ	k	α_0
0.15	-0.20	0.40	3.01252
0.15	-0.20	0.50	2.64497
0.15	-0.20	0.60	2.36857
0.15	-0.20	0.70	2.15551
0.15	-0.20	0.80	1.98812
0.15	-0.20	0.90	1.85469
0.15	-0.20	1.00	1.74715
0.15	-0.15	0.40	2.87767
0.15	-0.15	0.50	2.51782
0.15	-0.15	0.60	2.24720
0.15	-0.15	0.70	2.03856
0.15	-0.15	0.80	1.87455
0.15	-0.15	0.90	1.74369
0.15	-0.15	1.00	1.63808

h	Θ	k	α_0
0.15	0.00	0.40	2.49373
0.15	0.00	0.50	2.15556
0.15	0.00	0.60	1.90210
0.15	0.00	0.70	1.70718
0.15	0.00	0.80	1.55420
0.15	0.00	0.90	1.43218
0.15	0.00	1.00	1.33363

h	Θ	k	α_0
0.15	-0.10	0.40	2.74655
0.15	-0.10	0.50	2.39410
0.15	-0.10	0.60	2.12919
0.15	-0.10	0.70	1.92501
0.15	-0.10	0.80	1.76452
0.15	-0.10	0.90	1.63641
0.15	-0.10	1.00	1.53294
0.15	-0.05	0.40	2.61871
0.15	-0.05	0.50	2.27346
0.15	-0.05	0.60	2.01425
0.15	-0.05	0.70	1.81463
0.15	-0.05	0.80	1.65780
0.15	-0.05	0.90	1.53264
0.15	-0.05	1.00	1.43151

4.5 Albedo colour palette

The colour palette used in MSA publication is given in this Section.

Albedo range			rgb value					
0.000	-	0.020	(	0	,	0	,	050	)
0.020	-	0.040	(	0	,	0	,	100	)
0.040	-	0.050	(	0	,	0	,	200	)
0.050	-	0.060	(	0	,	0	,	255	)
0.060	-	0.070	(	80	,	20	,	10	)
0.070	-	0.080	(	100	,	30	,	20	)
0.080	-	0.090	(	100	,	50	,	30	)
0.090	-	0.100	(	80	,	60	,	40	)
0.100	-	0.110	(	60	,	80	,	40	)
0.110	-	0.120	(	20	,	80	,	20	)
0.120	-	0.130	(	30	,	100	,	30	)
0.130	-	0.140	(	40	,	120	,	40	)
0.140	-	0.150	(	50	,	140	,	50	)
0.150	-	0.160	(	60	,	160	,	50	)
0.160	-	0.170	(	80	,	180	,	30	)
0.170	-	0.180	(	100	,	160	,	20	)
0.180	-	0.190	(	110	,	150	,	10	)
0.190	-	0.200	(	120	,	140	,	10	)
0.200	-	0.210	(	140	,	120	,	0	)
0.210	-	0.220	(	130	,	110	,	0	)
0.220	-	0.230	(	125	,	99	,	0	)
0.230	-	0.240	(	120	,	80	,	0	)
0.240	-	0.250	(	111	,	75	,	0	)
0.250	-	0.260	(	120	,	82	,	7	)
0.260	-	0.280	(	126	,	91	,	14	)
0.280	-	0.300	(	141	,	108	,	28	)
0.300	-	0.325	(	156	,	125	,	42	)
0.325	-	0.350	(	171	,	142	,	56	)
0.350	-	0.375	(	186	,	159	,	71	)
0.375	-	0.400	(	201	,	176	,	85	)
0.400	-	0.450	(	216	,	193	,	99	)
0.450	-	0.500	(	231	,	210	,	113	)
0.500	-	0.550	(	240	,	220	,	120	)
0.550	-	0.600	(	246	,	225	,	135	)
0.600	-	0.650	(	246	,	235	,	155	)
0.650	-	0.700	(	240	,	240	,	180	)
0.700	-	0.750	(	250	,	250	,	210	)
0.750	-	0.800	(	230	,	253	,	200	)
0.800	-	0.900	(	220	,	230	,	240	)

5 MSA product format description

5.1 Overview

One MSA product contains surface albedos estimated in the Meteosat VIS band spectral range. One product generated every 10-day compositing periods. These compositing periods are defined with the Julian day number, *i.e.*, the first period runs from day 1 to 10, the second from day 11 to 20 and so on. The last period of the year is therefore slightly shorter than the other periods and runs from day 361 to 365[1].

The MSA product is not derived over the entire Meteosat disc and no sea mask is applied during the generation process so that values over sea are also available is this area. The spatial resolution of the MSA product is equal to the one of the Meteosat VIS band instrument. The distance between to adjacent pixels at the sub-satellite point is equal to 2.5 km.

[1] 366 for leap year.

5.2 Retrieving the MSA product from UMARF

The product can be ordered from EUMETSAT web page at the following URL:

http://archive.eumetsat.org/umarf/

Access to the product is only granted to registered users. In the list of products, the MSA product is identified as the MTP Mean Surface Albedo 0100. Make sure your select the format you want.

The MSA product is available in BUFR, HDF4 and HDF5 formats. Each format contains the same fields. Field names of the HDF format are described here. Each 10-day product is composted of three files:

- The first file contains the albedo values and its associated quality indicator
  e.g. `MSA_Albedo_L2.0_V2.01_000_2000_311_320.HDF`.
- The second one contains all the ancillary information
  e.g. `MSA_Ancillary_L2.0_V2.01_000_2000_311_320.HDF`.
- Finally, a static file contains the geographical location of each pixel
  e.g. `MSA_Static_L2.0_V2.1_0.HDF`.

5.3 The surface albedo product file

5.3.1 Naming convention

The filename has the following structure:
`MSA_Albedo_L2.0_V`*m.nn_sss_yyyy_fff_lll*`.HDF`
Where:

m	=	MSA algorithm major version number
nn	=	MSA algorithm minor version number
sss	=	Sub-satellite point code (000, 063,)
yyyy	=	four digit of the year
fff	=	First Julian day of the period
lll	=	Last Julian day of the period

5.3.2 Global attributes

`Nominal SSP`	Centre of the reference grid in the Meteosat projection.
`Start line`	The line number (row) of the first pixel of the datasets in the Meteosat projection for thevisible resolution (5000 $\times$ 5000 pixels). Indexing starts at 1.
`Height`	The y dimension of the datasets.
`Start pixel`	The pixel number (column) of the first pixel of the datasets in the Meteosat projection for the visible resolution (5000 $\times$ 5000 pixels). Indexing starts at 1.
`Width`	The x dimension of the datasets.
`HDF Conversion time`	Date and time when the HDF file has been generated.
`Satellite number`	The satellite identifier (in the range [1–7]).
`Start year`	The starting year (number) of the compositing period.
`Start Julian day`	Start Julian day of the period.
`End year`	The ending year (number) of the compositing period.
`End Julian day`	End Julian day of the period.
`Number of products`	The total number of valid pixels in each dataset.
`Actual Nbr Day`	The actual number of days in the compositing period (in the range [1–10]).
`MSA major version`	Version of the MSA algorithm
`MSA minor version`	Patch level of the major version number.
`Calibration version`	Version of the calibration datasets.
`Water Reflectance threshold`	Minimum TOA BRF below which observations have been rejected.
`Cloud for Sure threshold`	Maximum TOA BRF above which observations have been rejected.
`Cloud screening smooth`	TOA smoothness used for the cloud screening
`Probability alpha`	Confidence level for the error estimation
`Autocorrelation coefficient`	Coefficient α in Equation (16)
`Percent good pixels`	Percentage of pixels with a valid solution among the total number of processed pixels.
`Mean Relative Radiometric Error`	Mean relative radiometric error (Equation 5) in percent.
`Mean Number Slots`	Mean number of available observation per pixel prior to the cloud screening.

`Mean Number Processed Slots`	Mean value of N_y, the size of the measurement vector $\boldsymbol{y}_m$.
`Mean Valid Pixels`	Percentage of valid pixels.
`Mean Weak Solutions`	Percentage of pixels with a probability between 10 and 50%.
`Mean percent Dubious`	Percentage of pixels with a probability smaller than 10%.
`Mean percent no solutions`	Percentage of pixels with no solution
`Mean Optical Thickness`	Mean optical thickness
`Actual SSP latitude`	Mean value of the actual spacecraft SSP latitude.
`Actual SSP longitude`	Mean value of the actual spacecraft SSP latitude.
`Mean probability threshold`	Mean value of the probability $P_(\sigma_y)$.
`Mean DHR30`	Mean value of the DHR.
`Mean DHR30 relative error`	Mean value of the DHR relative error in percent.
`MSA version string`	MSA algorithm version number as a string.
`Start day`	The starting day of the month (number) of the compositing period.
`Start month`	The starting month (number) of the compositing period.
`End day`	The end day of the month (number) of the compositing period.
`End month`	The end month (number) of the compositing period.
`Start date string`	The starting day of the 10-day compositing period. The format is "dd/mm/yyyy" plus a space character, the letter "J" and a three digit number indicating the Julian day of the year.
`End date string`	The end date of the 10-day compositing period. The format is "dd/mm/yyyy" plus a space character, the letter "J" and a three digit number indicating the Julian day of the year.
`Period index`	The number obtained by dividing the ending Julian day by 10.
`Processing time`	Date and time when the product has been generated.
`Satellite generation`	Always "MET".

5.3.3 Scientific data set

Each SDS is a bi-dimensional matrix of pixels corresponding to an image in the Meteosat projection with the same East-West and South-North scanning mode. These values are are coded on one byte with the value 255 used to indicate invalid pixels. Decoded values are calculated as with DV = CAL * (CV - Offset) where DV is the decoded value and CV is stored value. CAL and OFFSET fields are available in the CALIBDATA HDF structure.

The conversion of the `DHR30` and `BHRiso` fields into broadband albedo is given in Section (4.3).

Name	Description	Symbol	Eq.
`BHRiso`	The isotropic Bi-Hemispherical Reflectance field contains the surface albedo in the Meteosat VIS band that would have been observed under isotropic illumination conditions for the best solution of day d with $\hat{\boldsymbol{x}}(d) = \bar{\hat{\boldsymbol{x}}}$ of the compositing period.	$\text{BHR}_\bullet$	32
`DHR30`	The Directional Hemispherical Reflectances field (`DHR30`) contains the surface albedo value for the best solution of day d with $\hat{\boldsymbol{x}}(d) = \bar{\hat{\boldsymbol{x}}}$ of the compositing period. It represents the "spectral albedo" in the Meteosat sensor VIS band spectral interval assuming a sun zenith angle of $\mu_0 = 30°$. Since the angle μ_0 is the same for all pixels along the year, the DHR is appropriate for the monitoring of the spatial or temporal changes of the surface radiative properties.	DHR	29
`DHR30 error 10D`	This field represents the estimated DHR error.	σ_{DHR}	30
`Probability (%)`	This field contains the probability of the solution $\hat{\boldsymbol{x}}$ of the selected day d of the compositing period. Pixels with a probability smaller than 80% or 90% should not considered when the MSA product is analysed.	$P_a(\hat{\boldsymbol{x}}(d))$	18

5.4 The ancillary data file

5.4.1 Naming convention

The filename has the following structure:

`MSA_Ancillary_L2.0_V`*m.nn_sss_yyyy_fff_lll*`.HDF`
Where:

m = MSA algorithm major version number
nn = MSA algorithm minor version number
sss = Sub-satellite point code (000, 063,)
yyyy = four digit of the year
fff = First Julian day of the period
lll = Last Julian day of the period

5.4.2 Global attributes

See Section (5.3.2).

5.4.3 Scientific data set

Each SDS is a bi-dimensional matrix of pixels corresponding to an image in the Meteosat projection with the same East-West and South-North scanning mode. These values are are coded on one byte with the value 255 used to indicate invalid pixels. Decoded values are calculated as with DV = CAL * (CV - Offset) where DV is the decoded value and CV is stored value. CAL and OFFSET fields are available in the CALIBDATA HDF structure.

Name	Description	Symbol	Eq.
QUALITY FLAG	This flag takes the following values: **Val Meaning** 0 Ok 1 No valid days in the period 2 No valid samples in the period 3 No likely day 4 Invalid solution index 5 Dubious solution, *i.e.*, $P_a(\hat{\boldsymbol{x}}(d)) = 0.1$ 6 Weak solution, *i.e.*, $0.1 < P_a(\hat{\boldsymbol{x}}(d)) \leq 0.5$		
NUMSOL	The number of acceptable solutions. The value 255 is set for invalid pixels.	$L_{\sigma_{\mathbf{y}}}$	24
NSLOT	Number of input slots before cloud screening.		
NSLOTASM	Number of clear sky input slots.	N_y	
K	Parameter describing the shape of the surface BRF in the RPV model for the best fit.	$\overline{\widehat{k}}$	

Name	Description	Symbol	Eq.
THETA	Parameter describing the assymetry of the surface BRF in the RPV model for the best fit.	$\overline{\widehat{\Theta}}$	
AER_OPT_THICK	Estimated equivalent aerosol optical thickness.	$\overline{\widehat{\tau}}$	
R0	Amplitude of the surface BRF in the RPV model for the best fit.	$\overline{\widehat{\rho}}_0$	
ERR_R0	Estimated error of $\overline{\widehat{\rho}}_0$.	$\sigma_{\overline{\widehat{\rho}}_0}$	27
NUMDAYS	Number of days with a solution during the compositing period.	N_T	
BESTDAY	Selected day during the compositing period.	d	
Chi2ASM	Normalised cost function of the best solution given by Equation (4), *i.e.*, χ^2/N_y.		
Chi2DCP	Cost function of the cloud screening.		
DHR Error	Estimated error of the DHR for the best day d.	σ_{DHR}	
ERR_K	Estimated error of	$\sigma\overline{\widehat{k}}$	27
ERR_T	Estimated error of	$\sigma_{\overline{\widehat{\Theta}}}$	27
ERR_OPT	Estimated error of	$\sigma_{\overline{\widehat{\tau}}}$	27
AVGOPT	Average value of $\hat{\tau}$ during the compositing period.		
ERR_AVG_ERR	Standard deviation of AVGOPT.		
RADIOMETRIC NOISE	Mean daily radiometric noise of the best day d calculated with $(\sum_{N_y} \sigma_y(t))/N_y$		

5.5 Static data set

5.5.1 Naming convention

The filename has the following structure:

MSA_Static_L2.0_V*m.nn_sss*.HDF
Where:

m = MSA algorithm major version number

nn = MSA algorithm minor version number

sss = Sub-satellite point code (000, 063,)

5.5.2 Global attributes

Contains a subset of the fields listed in Section (5.3.2).

5.5.3 Scientific data set

Name	Description	Symbol	Units	Min	Max	Scaled
`latitude`	Pixel latitude.	λ	degree	-90	+90	
`longitude`	Pixel longitude	ϕ	degree	0	360	

6 Algorithm change history

6.1 Changes in version 1.1

The following changes have been implemented in version 1.1 with respect to version 1.0:

1. The processed area over the zero degree mission has been increased.
2. A processing area over the 63°E mission has been defined.
3. The computation accuracy of the sun angles has been improved.
4. The computation of the viewing angles accounts now for the actual position of the spacecraft at the acquisition time.
5. The discretisation range of the predefined conditions for the $\widetilde{\tau}$, $\widetilde{k}$ and $\widetilde{\Theta}_{HG}$ parameters is now equal to:

$$\begin{aligned} \widetilde{\tau} &= \{0.1, 0.2, 0.4, 0.6, 1.0\} \\ \widetilde{k} &= \{0.5, 0.6, 0.7, 0.8, 0.9, 1.0\} \\ \widetilde{\Theta}_{HG} &= \{-0.3, -0.2, -0.1, 0.0\} \end{aligned}$$

6.2 Change in version 1.2

The following change has been implemented in version 1.2:

1. A error has been corrected in the access of the ECMWF total water column field.

6.3 Changes in version 2.1

Version 2.1 contains majors changes as it includes now an *a priori* estimation of the retrieval error of each parameter and the DHR.

1. The minimum number of slots is set to 6.
2. χ^2 is estimated are real χ^2 function.

3. The radiometric error is not prescribed anymore but is estimated for each pixel.
4. The retrieval mechanism accounts for the aerosol load autocorrelation during the day.
5. The threshold on the χ value is not prescribed anymore but calculated as a function of its probability.
6. The computation of the viewing angles accounts now for the actual position of the spacecraft at the acquisition time.
7. The error of the four retrieved parameters is estimated.
8. The 10-days compositing technique is based on a minimising of the error.
9. The discretisation range of the predefined conditions for the τ, $\widetilde{k}$ and $\widetilde{\Theta}_{HG}$ parameters is now equal to:

$$\begin{aligned} \tau &= \{0.1, 0.2, 0.4, 0.6, 0.8, 1.0\} \\ \widetilde{k} &= \{0.5, 0.6, 0.7, 0.8, 0.9, 1.0\} \\ \widetilde{\Theta}_{HG} &= \{-0.30, -0.25, -0.20, -0.15, -0.10, -0.05, 0.0\} \end{aligned}$$

References

Engelsen, O., B. Pinty, M. Verstraete, and J. Martonchik (1996, 1996). Parametric bidirectional reflectance factor models: evaluation, improvements and applications. Technical Report EUR 16426 EN, Space Applications Institute, JRC.

Govaerts, Y., M. Clerici, and N. Clerbaux (2004). Operational calibration of the Meteosat radiometer VIS band. *IEEE Transactions on Geoscience and Remote Sensing 42*(9), 1900–1914.

Govaerts, Y. and A. Lattanzio (2007). Retrieval error estimation of surface albedo derived from geostationary large band satellite observations: Application to Meteosat-2 and -7 data. *Journal of Geophysical Research 112*(D05102), doi:10.1029/2006JD007313.

Govaerts, Y., J. Pereira, B. Pinty, and B. Mota (2002). Impact of fires on surface albedo dynamics over the African continent. *Journal of Geophysical Research 107*(D22), doi:10.1029/2002JD002388.

Govaerts, Y., B. Pinty, M. Taberner, and A. Lattanzio (2006). Spectral conversion of surface albedo derived from Meteosat first generation observations. *Geosciences and Remote Sensing Letters*, 23–27 doi : 10.1109/LGRS.2005.854202.

Govaerts, Y. M. (1999). Correction of the Meteosat-5 and -6 VIS band relative spectral response with Meteosat-7 characteristics. *International Journal of Remote Sensing 20*(18), 3677–3682.

Holben, B., T. Eck, I. Slutsker, D. Tanre, J. Buis, A. Setzer, E. Vermote, J. Reagan, Y. Kaufman, T. Nakajima, F. Lavenu, I. Jankowiak, and A. Smirnov (1998). AERONET-a federated instrument network and data archive for aerosol characterization. *Remote Sensing of Environment 66*, 1–16.

Lattanzio, A., Y. Govaerts, and B. Pinty (2006). Consistency of surface anisotropy characterization with Meteosat observations. *Advanced Space Research*, doi:10.1016/j.asr.2006.02.049.

Loew, A. and Y. Govaerts (2010). Towards multidecadal consistent meteosat surface albedo time series. *Remote Sensing 2*(4), 957–967.

McPeters, R. (1996). Nimbus 7 Total Ozone Mapping Spectrometer (TOMS) data product's guide. Technical Report NASA Reference Publication 1384, NASA.

Pinty, B., F. Roveda, M. M. Verstraete, N. Gobron, Y. Govaerts, J. V. Martonchik, D. J. Diner, and R. A. Kahn (2000a). Surface albedo retrieval from Meteosat: Part 1: Theory. *Journal of Geophysical Research 105*, 18099–18112.

Pinty, B., F. Roveda, M. M. Verstraete, N. Gobron, Y. Govaerts, J. V. Martonchik, D. J. Diner, and R. A. Kahn (2000b). Surface albedo retrieval from Meteosat: Part 2: Applications. *Journal of Geophysical Research 105*, 18113–18134.

Rahman, H., B. Pinty, and M. M. Verstraete (1993). Coupled surface-atmosphere reflectance (CSAR) model. 2. Semiempirical surface model usable with NOAA Advanced Very High Resolution Radiometer data. *Journal of Geophysical Research 98*(D11), 20,791–20,801.